FULL PAPERS
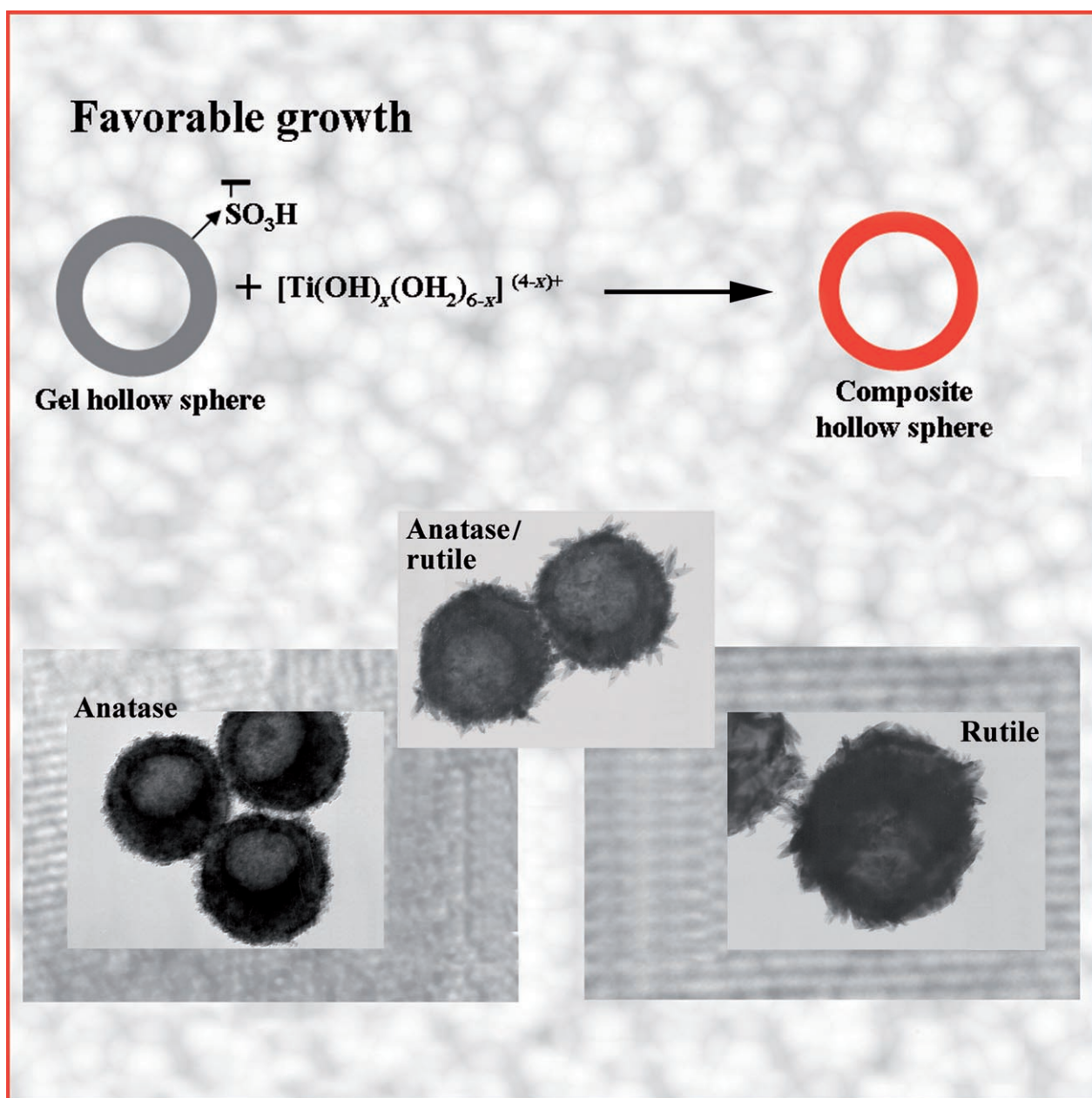
Low-Temperature Facile Template Synthesis of Crystalline Inorganic Composite Hollow Spheres

Huifang Xu,[a] Wei Wei,[a] Chengliang Zhang,[a] Shujiang Ding,[a] Xiaozhong Qu,[a] Jiguang Liu,[a] Yunfeng Lu,[b] and Zhenzhong Yang*[a]

Abstract: This report presents a facile approach for the low-temperature synthesis of crystalline inorganic-oxide composite hollow spheres by employing the bulk controlled synthesis of inorganic-oxide nanocrystals with polymer spheres as templates. The sulfonated polystyrene gel layer can adsorb the target precursor and induce inorganic nanocrystals to grow on the template in situ. The crystalline phase and morphology of the composite shell is tunable. By simply adjusting the acidity of the titania sol, crystalline titania composite hollow spheres with tunable crystalline phases of anatase, rutile, or a mixture of both were achieved. The approach is general and has been extended to synthesize the representative perovskite oxide (barium and strontium titanate) composite hollow spheres.

Keywords: hollow spheres · nanocrystals · perovskite phases · sol–gel processes · template synthesis

The traditional thermal treatment for crystallite transformation is not required, thus intact shells can be guaranteed. The combination of oxide properties such as high refractive index, high dielectric constant, and catalytic ability with the cavity of the hollow spheres is promising for applications such as opacifiers, photonic crystals, high-κ-gate dielectrics, and photocatalysis.

Introduction

Inorganic coated-polymer core–shell composites and the corresponding hollow spheres have attracted growing interest due to their potential applications in catalysis, controlled delivery, artificial cells, light-weight fillers, thermal and acoustic insulation, and photonic crystals.[1,2] Such spheres are usually prepared by controlled coating onto template core particles, which is usually assisted by layer-by-layer deposition.[3,4] The shells can be made of polymeric, biological, metallic, or inorganic materials.[5–9] Among these hollow spheres, inorganic-oxide hollow spheres have outstanding physical and chemical properties, and are therefore promising in various applications, for example, as photocatalysts, photovoltaic cells, opacifiers in paints, UV absorbers in cosmetics, and dielectric ceramics.[10–16] The properties of these hollow spheres are mainly determined by their crystallographic phases. For action as an opacifier, enhancement of the refractive index n of the shell is necessary to scatter visible light effectively.[17] Crystalline titania (TiO_2) has n values of 2.5–2.7 depending on the crystalline phase; these values are much higher than those of the commonly used polymer and silica shells ($n = 1.4$–1.6).[18] Among the inorganic oxides, barium titanate ($BaTiO_3$) or strontium titanate ($SrTiO_3$) with the perovskite phase has a high dielectric constant $K \approx 10^2$–10^3.[19]

Many methods have been proposed for the synthesis of these hollow spheres based on templates, such as the sol–gel, coprecipitation, and layer-by-layer assisted-deposition approaches.[20–28] Templates can be hard particles, gel particles, or hollow spheres. Notably, in these methods, the inorganic-oxide shells prepared are usually amorphous. A subsequent high-temperature thermal treatment is required to transform the amorphous oxide shells into crystallites. The crystallization and further growth of the oxide particles usually leads to a deterioration of the shell and a tendency for perforation and fragmentation. In particular, when the production of rutile TiO_2 hollow spheres was attempted at high temperatures, the shell structure completely disappeared.[23,26]

The conventional sol–gel process usually involves uncontrollable fast hydrolysis and condensation, and therefore can result in the formation of amorphous inorganic oxides.[23–27,29,30] It is thus necessary to synthesize crystalline inorganic oxides under mild conditions. Recently, there have been some reports on the direct synthesis of inorganic-oxide nanocrystals under mild conditions simply by controlling the thermodynamic factors during the reaction. For example, as protons can slow down condensation in the acid-catalyzed sol–gel process, TiO_2 nanocrystals with tunable crystalline phases were synthesized at low temperatures.[31–33] Similarly, $BaTiO_3$ and $SrTiO_3$ nanocrystals were also prepared at low temperatures.[34–36]

In this paper, we combined the bulk controlled facile synthesis of inorganic nanocrystals with the synthetic method

[a] H. Xu, W. Wei, C. Zhang, S. Ding, Dr. X. Qu, Dr. J. Liu, Prof. Z. Yang
State Key Laboratory of Polymer Physics and Chemistry
Institute of Chemistry
Chinese Academy of Sciences, Beijing 100080 (China)
Fax: (+86) 10-62559373
E-mail: yangzz@iccas.ac.cn

[b] Prof. Y. Lu
Department of Chemical and Biomolecular Engineering
University of California at Los Angeles
Los Angeles, CA 90095-1592 (USA)

FULL PAPERS

based on sphere templates. The crystalline inorganic-oxide composite and the corresponding hollow spheres were prepared under mild conditions. This method avoids the thermal treatment, which is usually required to transform amorphous oxides into crystalline ones during traditional template synthesis. Thus, our method guarantees intact shells. The sulfonated-polystyrene (PS)-gel layer of the template can adsorb the target precursor and induce inorganic nanocrystals to grow in situ on the template. The method is facile and general for many crystalline inorganic oxides such as TiO_2, as well as perovskite-phase mixed metal oxides such as $BaTiO_3$ and $SrTiO_3$.

Results and Discussion

TiO$_2$/Polymer Composite Spheres and the Corresponding Hollow Spheres

As a first proof of the approach, crystalline TiO_2 composite and the corresponding hollow spheres were synthesized at low temperature. To synthesize crystalline TiO_2 composite hollow spheres in situ without removal of the polymer cores, sulfonated-PS-gel hollow spheres[24,25] were used as templates. The parent polymer hollow spheres are mainly composed of a linear-PS-shell skeleton. To strengthen the polymer shell, swelling radical polymerization of styrene/divinylbenzene was carried out within the parent PS shell at 80 °C. The weight ratio of monomer styrene/divinylbenzene mixture (1:1 *w/w)* to parent PS hollow spheres was 1:1. A series of gel spheres were prepared by sulfonation of the cross-linked-PS hollow spheres with concentrated sulfuric acid. The thickness of the gel layer was controlled by the sulfonation temperature and time.[24,25] Two representative gel hollow spheres S1 and S2 were derived accordingly by sulfonation at 40 °C for 1 and 3 h, respectively. The average shell thickness of hollow spheres S1 was about 100 nm. With the sulfonation time prolonged to 3 h, hollow spheres S2 were prepared with thicker shells of about 120 nm. Elemental analysis shows that the S1 and S2 spheres contain 2.30 and 3.66 wt % of sulfur atoms, respectively. Both gel spheres are hollow with the spherical contour well-preserved (Figure 1). In comparison, gel spheres derived from linear-PS hollow spheres were distorted or collapsed and lost their spherical
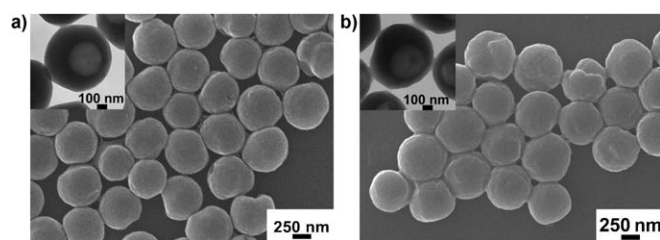

Figure 1. SEM and TEM (inset) images of two representative gel hollow spheres with varying degrees of sulfonation. a) S1, b) S2.

contour after drying;[24] this poses problems for the preparation of hollow spheres. Thus, cross-linked-gel hollow spheres were used in our study. The derived sulfonic acid and sulfone groups were detected by FTIR spectroscopy (Figure 2).
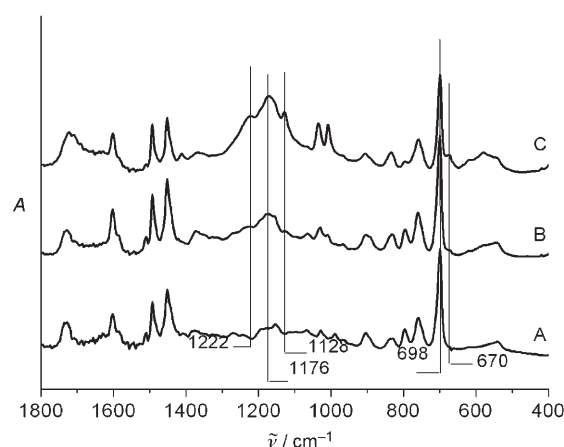

Figure 2. FTIR spectra of three representative polymer hollow spheres. A) Cross-linked-PS hollow spheres. B) and C) Sulfonated-PS-gel spheres S1 and S2 after the PS sphere was sulfonated for 1 and 3 h, respectively.

The characteristic band at 1128 cm^{-1} is related to the sulfone group ($-SO_2-$). The bands at 670, 1176, and 1222 cm^{-1} are assigned to the derived sulfonic acid group (SO_3H). With the sulfonation time further prolonged, the degree of sulfonation was increased until the whole shell was in gel form.

In this study, S1 spheres with a thin sulfonated PS layer were selected as the template for preparing the crystalline TiO_2 composite hollow spheres. pH control to a relatively low value (pH < 2) is crucial to facilitate the formation of crystalline TiO_2.[31–33] The growing crystalline TiO_2 species such as $[Ti(OH)_x(OH_2)_{6-x}]^{(4-x)+}$ are positively charged,[31] as pH < 2 is lower than the isoelectric point of TiO_2 (pH 5–7).[37] Thus, the negatively charged sulfonic acid groups of the template adsorb the positively charged growing crystalline TiO_2 species, which induces the TiO_2 nanocrystals to grow onto the template in situ. At an initial pH value of the TiO_2 sol of 1.5, anatase/S1 composite hollow spheres with coarse surfaces were obtained (Figure 3a and b). The Brunauer–Emmett–Teller (BET) surface area increased from 11.1 m^2 g^{-1} of the template to 30.4 m^2 g^{-1} of the composite

Abstract in Chinese：

利用本体低温制备无机氧化物纳米晶的方法，与微球模板合成技术结合，提出一步低温制备了结晶无机氧化物 - 高分子复合及相应的中空微球。模板中的磺化聚苯乙烯凝胶层对吸附无机氧化物纳米晶的前驱体，以及对诱导无机氧化物纳米晶在模板上的优先原位生长具有决定作用。控制反应体系的酸碱度，在温和条件下便可分别制备锐钛矿型、金红石型及两者混合的二氧化钛复合中空微球。此方法具有普适性，进一步扩展制备了钙钛矿型如钛酸钡、钛酸锶的中空微球。本方法避免了晶型转化和去除模板所需的高温处理步骤，能充分保证结晶无机氧化物中空微球的壳层保持完整不破裂。结晶无机物的特性如高折射率、高介电常数和催化性能与中空微球的空腔结构相结合，将产生新性质，为其新应用奠定基础。
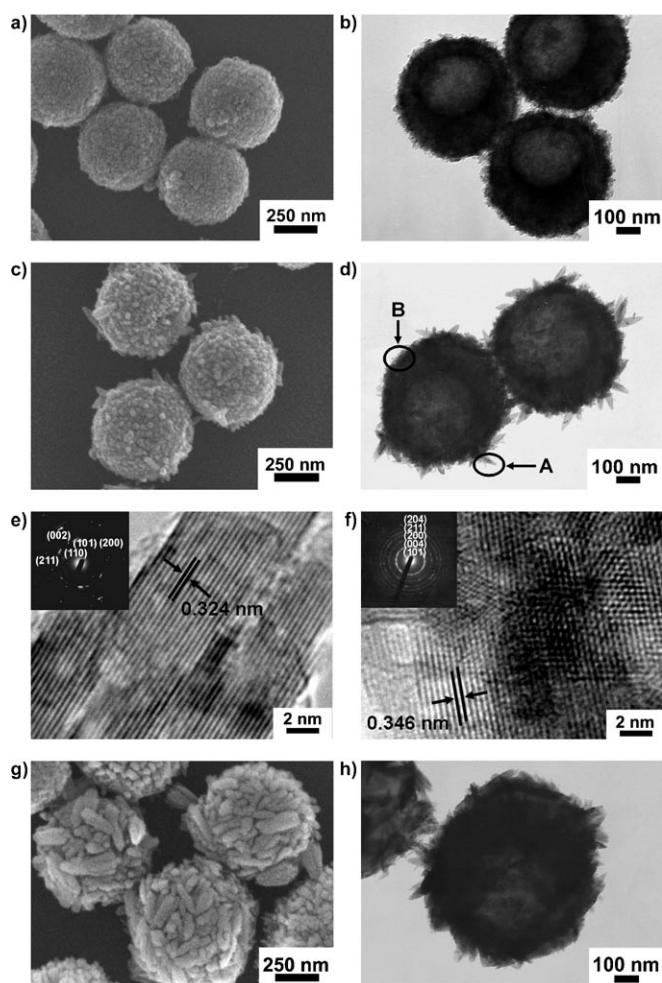
Figure 3. a) and b) SEM and TEM images, respectively, of anatase/S1 composite hollow spheres. c) and d) SEM and TEM images, respectively, of anatase/rutile/S1 composite hollow spheres. e) and f) HRTEM images of regions A and B, respectively, of the sample shown in d); inset: SAED patterns in which the rutile and anatase phases are confirmed, respectively. g) and h) SEM and TEM images, respectively, of rutile/S1 composite hollow spheres.

Figure 4. XRD patterns of titania/S1 composite hollow spheres a) before and b) after calcination in air at 450 °C for 2 h. Samples A, B, and C were prepared with increasing acidity of the starting sols. A: pH 1.5; B: pH 0.5; C: $[H^+] = 1.5$ M. $\triangledown$ = rutile (JCPDS No. 21-1276), $\bullet$ = anatase (JCPDS No. 21-1272).

hollow sphere. Compared with the template, the diameter of the composite hollow spheres increased by about 30 nm. The anatase phase was verified by high-resolution TEM (HRTEM), selected area electron diffraction analysis (SAED), and XRD (Figure 4a, pattern A). The rutile phase gradually appeared with increasing acidity of the starting sol. As an example, at pH 0.5, the representative composite spheres were obtained with anatase/rutile phases coexisting (Figure 4a, pattern B). The anatase/rutile ratio was 4:3 calculated according to the main-peak intensity.[38] The BET surface area was 21.6 m^{2}g^{-1}, and the TiO$_2$ content was 36.9 wt% measured by thermogravimetric analysis (TGA). The TiO$_2$ content could be controlled by the feed amount of the starting sol. However, an excess of the sol led to the formation of TiO$_2$ in the continuous media and even to aggregation among the composite spheres. S2 hollow spheres with thicker gel layers were used as the template to increase
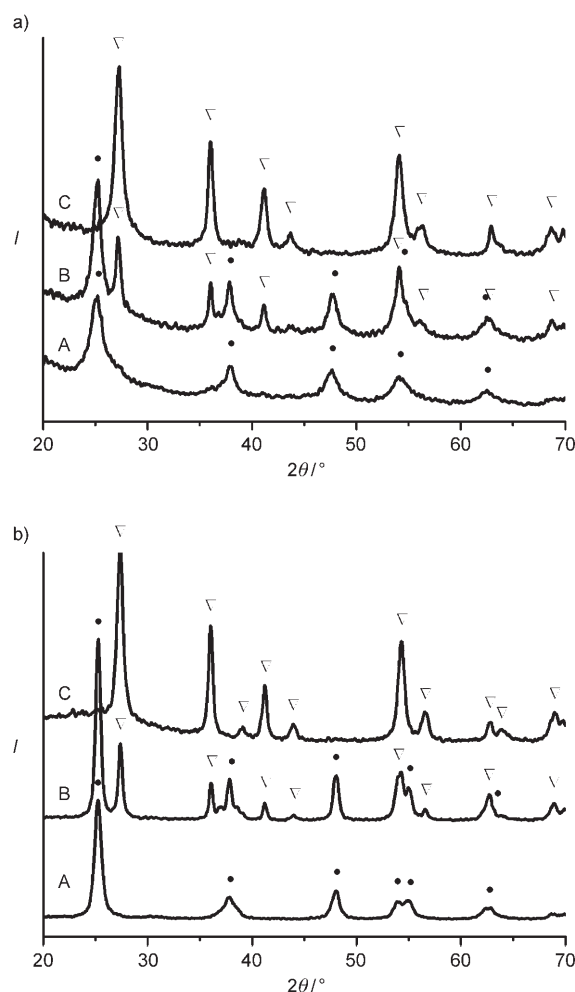
TiO$_2$ content further. TiO$_2$ content was increased from 36.9 wt% of TiO$_2$/S1 to 45.5 wt% of TiO$_2$/S2. Figure 3c and d shows, on the anatase coarse surface, the growing and protruding nanosized needles. The composite spheres have two distinct regions in morphology, labeled A and B (Figure 3d). HRTEM (Figure 3e) reveals that the needles of region A are of rutile phase with a (110) lattice spacing of 0.324 nm, and region B, which corresponds to the coarse surface, is identified as anatase phase, with a (101) lattice spacing of 0.346 nm (Figure 3f). The SAED pattern in Figure 3e, inset shows that the fringe patterns with spacings of 0.324, 0.248, 0.229, 0.168, and 0.148 nm correspond to the rutile (110), (101), (200), (211), and (002) spacings, respectively. In the SAED pattern in Figure 3f, inset, the five fringe patterns with spacings of 0.346, 0.238, 0.186, 0.164, and 0.145 nm are consistent with the anatase (101), (004), (200), (211), and (204) spacings. SEM and XRD results provide further information on morphology and crystalline-phase evolution with

FULL PAPERS

the prolonged sol–gel process. During the initial stage, heterogeneous nucleation onto the gel spheres dominated following the gradual growth of anatase. With further prolonging, the rutile phase started to grow onto the anatase surface. The rutile phase fraction was increased at lower temperature at the given pH value. However, both methods are time-consuming for obtaining more rutile phase. Alternatively, when the acid concentration of starting sol was further increased to 1.5 M, rutile/S1 composite spheres were obtained with needles predominantly grown (Figure 3 g and h). The hollow cavity of the rutile/polymer composite spheres is discerned from the TEM image (Figure 3 h). After the composite spheres were calcinated at 450 °C in air to remove the polymers, the characteristic bands attributed to the sulfonic acid and sulfone groups completely disappeared, which is confirmed by FTIR spectroscopy (not shown). X-ray photoelectron spectroscopy (XPS) (see Supporting Information, Figure S1) further indicates that some sulfur exists in the form of S^{VI}, which may be attributed to sulphate.[39] Energy-dispersive X-ray analysis (EDX) gives the atomic ratio of Ti/S as 38.4:1. By assuming complete formation of the sulphate $Ti(SO_4)_2$, the maximum content of sulphate was estimated to be 3.9 wt % in the TiO_2 hollow spheres. The calcination has less effect on the morphology and crystalline fraction of the hollow spheres (Figure 4 b; see also Supporting Information, Figure S2). In comparison, the spherical contours completely disappeared when the amorphous TiO_2 composite spheres were calcinated at 900 °C to obtain rutile TiO_2 hollow spheres.[26] The XRD peaks became sharper, thus indicating further crystallization of TiO_2. This is consistent with the TEM results. Controlling the acidity of the starting sol determines the crystalline phase of TiO_2 grown on the gel template, which follows the same mechanism of formation of TiO_2 nanocrystals in the bulk.[31–33] In comparison, amorphous TiO_2 was grown when sol at pH 7 was used. When PS hollow spheres without sulfonation were used as templates, TiO_2 formed only in the continuous media.

Besides gel-hollow-sphere templates, sulfonated-PS core–shell gel solid spheres S3[26] were also used as template to synthesize crystalline TiO_2/polymer composite core–shell spheres. Similarly, anatase/S3 composite spheres of about 300 nm in diameter with coarse surfaces were formed at pH 1.5 (Figure 5 a). Hollow spheres with a cavity diameter of 250 nm and shell thickness of 25 nm were obtained after dissolution of the PS cores with N,N-dimethylformamide (DMF). A trace of sulfonated-PS gel was detected (Figure 6). After calcination at 450 °C in air, the template was removed (Figure 6, curve D). The shells of the composite hollow spheres are composed of nanoparticles about 10 nm in size (Figure 5 a, inset), which are of anatase phase as verified by HRTEM, SAED (similar to Figure 3 f), and XRD (similar to Figure 4 a, pattern A). At pH 0.7, composite spheres were prepared with coexisting anatase/rutile phases (similar to Figure 4 a, pattern B). The anatase/rutile ratio was 4:1 calculated according to the main-peak intensity.[38] On the anatase coarse surface, protruding nanosized needles grew (Figure 5 b). Hollow spheres were obtained
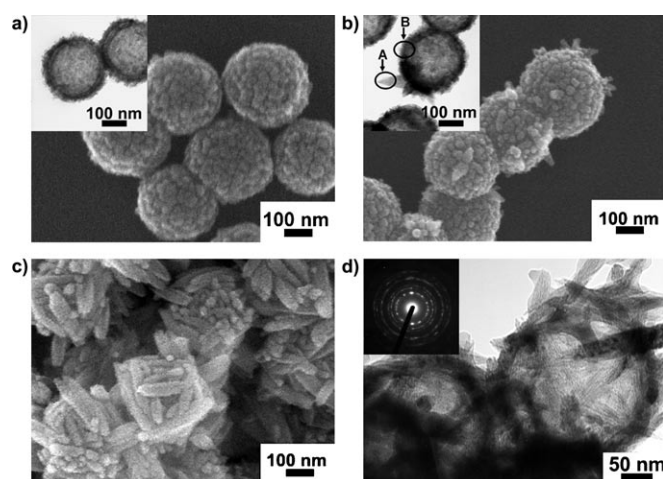

Figure 5. a) SEM image of anatase/S3 composite; inset: TEM image of the corresponding hollow spheres. b) SEM image of anatase/rutile/S3 composite; inset: TEM image of the corresponding hollow spheres. c) SEM image of rutile/S3 composite spheres. d) TEM image of the rutile hollow spheres; inset: SAED pattern indicates that the needles are randomly oriented. All the hollow spheres were prepared by dissolution of the PS cores in DMF.
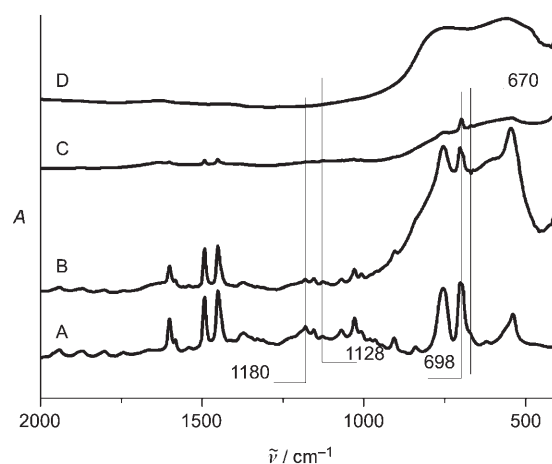

Figure 6. FTIR spectra of sulfonated-PS-gel spheres S3 (A), anatase/rutile/S3 composite spheres (B), anatase/rutile hollow spheres after template was removed by DMF (C), and anatase/rutile hollow spheres after calcination in air at 450 °C for 2 h (D). Most of the polymers in C were removed with a trace of gel left. For D, the polymers were completely removed.

after the cores were dissolved by DMF (Figure 5 b, inset). The two distinct regions labeled A and B were identified as rutile and anatase phase, respectively, by HRTEM and SAED analyses. Rutile/S3 composite spheres were formed with needles predominantly grown when the acid concentration of the starting sol was further increased to 1.5 M (Figure 5 c). Hollow spheres were formed after the PS cores were dissolved (Figure 5 d) (similar to Figure 4 a, pattern C); the spheres are composed of randomly oriented rutile needles (Figure 5 d, inset).

The above procedure was applied to a larger example of sulfonated-PS-gel spheres, S4 ($\approx 4\ \mu$m in diameter), for easy separation of the spheres by precipitation under gravity. At a relatively low pH value of 0.5, anatase/rutile/S4 composite spheres were prepared with protruding needles. After the PS cores were dissolved, hollow cavities were found in the occasionally broken spheres (Figure 7a). The coexistence of
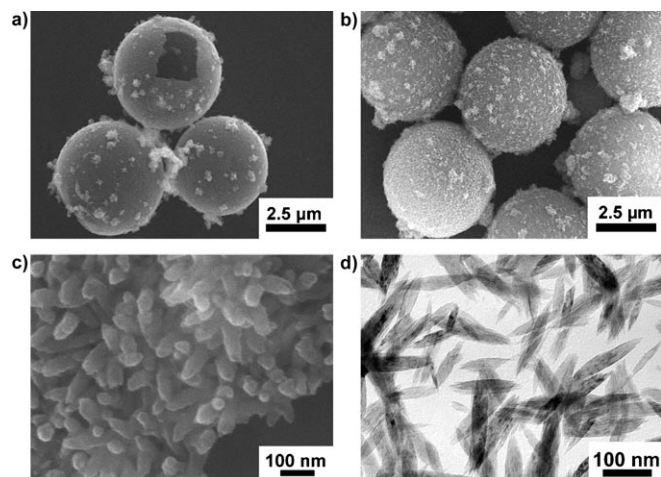

Figure 7. a) SEM image of anatase/rutile hollow spheres. b) SEM image of rutile/S4 composite spheres. c) Magnified SEM image of a hollow rutile sphere. d) TEM image of rutile needles obtained by drying the dispersion in ethanol.

anatase/rutile phases was verified by HRTEM, SAED, and XRD. Rutile/S4 composite spheres were prepared, whose outer surfaces are coarser with flowerlike structures (Figure 7b). The TiO$_2$ content was 23.8 wt % as measured by TGA. A magnified image (Figure 7c) of one of the hollow spheres reveals that the "flowers" are composed of nanosized rutile needles. Rutile needles 10^2 nm in length and 10^1 nm in diameter were prepared after the hollow spheres were broken by vigorous sonication. The needles were well-dispersed in solvent (Figure 7d). By changing the reaction parameters, the size and aspect ratio of the rutile particles could be controlled. In comparison, aggregates of the nanosized needles were usually obtained in the absence of template.

BaTiO$_3$ and SrTiO$_3$/Polymer Composite Spheres and the Corresponding Hollow Spheres

The sulfonated gel layer can also adsorb some precursors for the sol–gel process and further react with alkaline-earth metals to form perovskite inorganic nanocrystals under mild conditions. Gel hollow spheres S2 were used as the template to increase inorganic-oxide content so as to form intact composite hollow spheres. Tetrabutyl titanate (TBT) absorbed template S2 further reacted in the corresponding solution of alkaline-earth metal to form BaTiO$_3$ or SrTiO$_3$/S2 composite hollow spheres. As shown in Figure 8a and b, the shell is
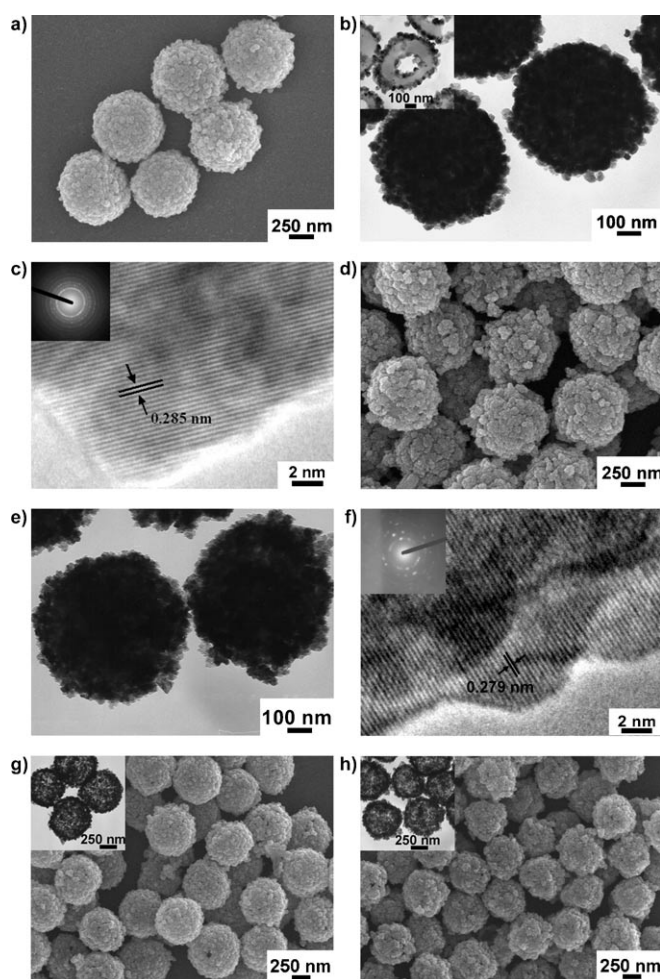

Figure 8. a) and b) SEM and TEM images, respectively, of BaTiO$_3$/S2 composite hollow spheres; inset of b): microtome image. c) HRTEM image of a typical particle on the shell of BaTiO$_3$/S2 composite hollow spheres; inset: SAED image. d) and e) SEM and TEM images, respectively, of SrTiO$_3$/S2 composite hollow spheres. f) HRTEM image of a typical particle on the shell of SrTiO$_3$/S2 composite hollow spheres; inset: SAED image. g) SEM and TEM (inset) images of BaTiO$_3$ hollow spheres obtained after BaTiO$_3$/S2 composite hollow spheres were calcinated in air at 450 °C. h) SEM and TEM (inset) images of SrTiO$_3$ hollow spheres obtained after SrTiO$_3$/S2 composite hollow spheres were calcinated in air at 450 °C.

composed of BaTiO$_3$ nanoparticles about 30 nm in diameter. The BaTiO$_3$ content was 59.4 wt % as determined by TGA. The representative microtome TEM image (Figure 8b, inset) indicates that the composite spheres preserved their hollow structure, and BaTiO$_3$ grew on both interior and exterior gel surfaces. This is similar to our previous results,[24,25] which revealed that the gel shell has a sandwich structure. The HRTEM image of the nanoparticles (Figure 8c) shows the (110) lattice spacing of 0.285 nm, which corresponds to cubic BaTiO$_3$. This is confirmed by the SAED image in the inset and the XRD pattern (Figure 9a, pattern A), which is consistent with JCPDS No. 31-0174. The average crystal size was estimated to be about 23.7 nm by the Scherrer equation,[40] consistent with the SEM and TEM results. Similarly,
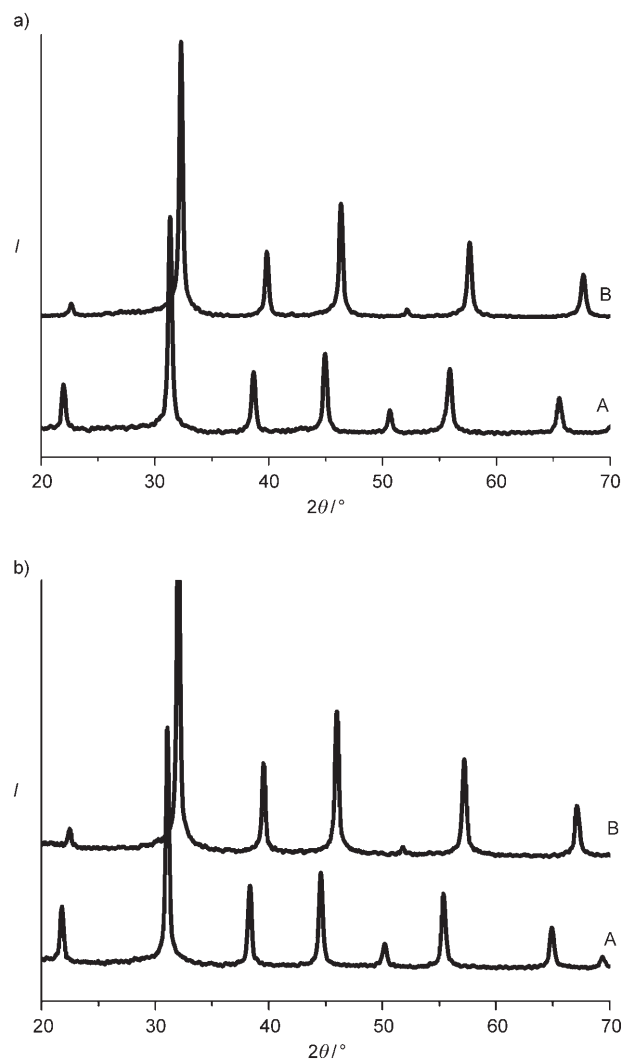
a)

b)

Figure 9. XRD patterns of BaTiO$_3$ and SrTiO$_3$/S2 composite hollow spheres a) before and b) after calcination in air at 450 °C. Pattern A: cubic BaTiO$_3$ (JCPDS No. 31-0174). Pattern B: cubic SrTiO$_3$ (JCPDS No. 35-0734).

a)

b)

Figure 10. EDX results of the two representative composite hollow spheres. a) BaTiO$_3$/S2; b) SrTiO$_3$/S2. The Pt and Si peaks are attributed to the grid. The C and S peaks are from the template.

SrTiO$_3$ composite hollow spheres were also synthesized (Figure 8 d and e). The SrTiO$_3$ content was 47.5 wt %. The HRTEM image (Figure 8 f) shows the (110) lattice spacing of 0.279 nm, which is confirmed by SAED to be the cubic phase (Figure 8 f, inset). The XRD pattern (Figure 9 a, pattern B) is consistent with JCPDS No. 35-0734. The average crystal size is estimated to be about 24.2 nm by the Scherrer equation, consistent with the electron microscopy results. EDX analysis (Figure 10) indicates the presence of Ba or Sr, Ti, and O in the composite hollow spheres. Further analysis of the EDX results reveals that the Sr/Ti ratio is 1.08:1. This is very close to the stoichiometric Sr/Ti ratio of 1:1 in SrTiO$_3$. In the case of BaTiO$_3$, as there is an overlap between the Ba L edge and the Ti K edge in the energy range 4.5–5 keV, it is difficult to distinguish each edge to determine quantitatively each composition. This was also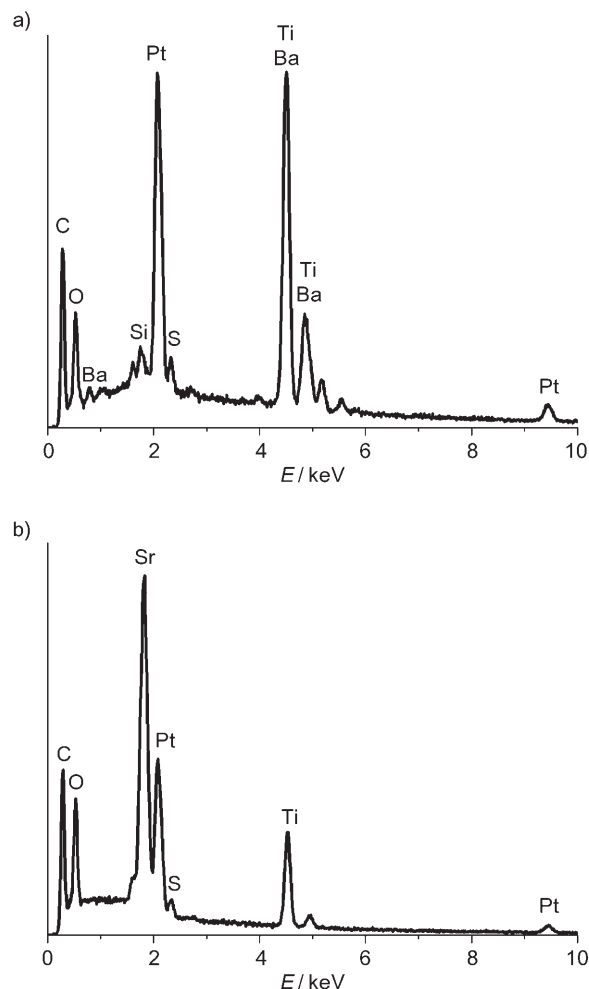 discussed by another report.[41] Polymer templates were re-moved by calcination at 450 °C in air for 2 h. The corresponding BaTiO$_3$ and SrTiO$_3$ hollow spheres were obtained (Figure 8 g and h). The hollow cavity structure was clearly observed because of the removal of the template. However, the BaTiO$_3$ or SrTiO$_3$ shell is still intact. The diameter of the hollow spheres is less changed than that of the composite spheres. The crystallinity is also less influenced, as verified by XRD (Figure 9 b). This indicates that calcination has less effect on the morphology and crystallinity of the hollow spheres. When PS hollow spheres without sulfonation were used as template, some BaTiO$_3$ or SrTiO$_3$ particles formed only in the continuous media. This implies that the sulfonated-PS-gel layer plays a key role in adsorbing TBT and inducing BaTiO$_3$ or SrTiO$_3$ to grow on the template in situ. On the other hand, in relation to the control experiment of synthesizing crystalline BaTiO$_3$ or SrTiO$_3$ in the bulk, we also found that the sulfonated-PS-gel layer has little influence on the crystallization of BaTiO$_3$ or SrTiO$_3$.

Conclusions

We have proposed a facile method to synthesize a series of crystalline inorganic-oxide/polymer composite and the corresponding hollow spheres. The sulfonated-PS-gel layer can adsorb the reactive precursor and induce inorganic-oxide nanocrystals to grow on the template in situ. The crystalline phase and morphology of the composite shell is tunable. By simple adjustment of the acidity of the TiO_2 sol, crystalline TiO_2 composite hollow spheres composed of anatase, rutile, or a mixture of both can be produced with tunable crystalline phases. Moreover, we have also synthesized composite hollow spheres of the representative perovskite oxides such as $BaTiO_3$ and $SrTiO_3$ at low temperature. In our approach, thermal treatment at high temperature for crystallite transformation is avoided, thus the spherical contour of the hollow spheres can be better preserved. The combination of oxide properties such as high refractive index, high dielectric constant, and catalytic ability with the cavity of the hollow spheres is promising for applications such as opacifiers, photonic crystals, high-κ-gate dielectrics, and photocatalysis.

Experimental Section

Syntheses

Sulfonated-PS-gel-sphere templates:[24–26] Gel templates were prepared by sulfonation of the corresponding PS spheres of various sizes. Freeze-dried PS spheres were dispersed into a large amount of concentrated sulfuric acid at 40 °C for different times to control the thickness of the sulfonated-PS-gel layers. The two representative gel templates S1 and S2 were prepared by sulfonation of the corresponding cross-linked-PS hollow spheres of about 500 nm in diameter for 1 and 3 h, respectively; S3 and S4 were prepared by sulfonation of PS solid spheres 250 nm and 4 μm in diameter, respectively, for 1 h. The sulfonated-PS-gel spheres were washed with water/ethanol.

TiO_2/polymer composite and the corresponding hollow spheres: Titanium isopropoxide (TTIP) was used as precursor. To obtain the composite spheres without forming TiO_2 in the continuous media, the TTIP concentration was controlled at 0.01–0.05 M depending on the degree of sulfonation and type of template. Nitric acid was used to adjust the acidity for the prolonged sol–gel process. The reaction temperature was controlled at 40–75 °C. A typical procedure is as follows: TTIP (0.1 mL), isopropyl alcohol (1.5 mL), and nitric acid (2 M, 4.5 mL) were mixed under stirring at room temperature for 1 h to form a concentrated transparent sol. By adding distilled water to the sol until a final volume of 25 mL, the final sol of pH 0.5 was obtained for use. S1 (50 mg) was added to the above sol (25 mL) under stirring for 2 h so that the sol was absorbed into the sulfonated-PS-gel layer. The dispersion was then heated at 65 °C for 24 h under stirring to form anatase/rutile/S1 composite spheres. The anatase/rutile ratio was 4:3 calculated according to the main-peak intensity.[38] The acidity of the sol was adjusted by altering the feed amount of nitric acid to change the crystalline phase from anatase to rutile. At the initial pH of the TiO_2 sol of 1.5, anatase/S1 composite hollow spheres were prepared. When the acid concentration of the sol was increased to 1.5 M, rutile/S1 composite hollow spheres were obtained. The composite hollow spheres were separated by centrifugation and then washed with ethanol/water. Polymer templates were removed either by dissolution with DMF or by calcination in air at 450 °C for 2 h.

$BaTiO_3$ or $SrTiO_3$/polymer composite and the corresponding hollow spheres: A typical procedure is as follows: S2 (50 mg) was dispersed into a mixture of absolute ethanol and TBT (1:1 v/v, 2 mL) for 24 h. The TBT-adsorbed spheres were washed with absolute ethanol twice and then treated with $Ba(OH)_2$ or $Sr(OH)_2$ (0.3 M, 4 mL) at 70 °C for 12 h under stirring. After the reaction was completed, the white precipitate was separated by centrifugation and then washed with distilled water. The polymer templates were removed by calcination in air at 450 °C for 2 h.

Characterization

The spheres were dispersed in ethanol and spread onto carbon-coated copper grids for TEM (JEOL 100CX operating at 100 kV). HRTEM and SAED analysis were performed with a HITACHI H-9000NAR electron microscope operating at 300 kV. SEM and EDX analysis was performed with a HITACHI S-4300 instrument operating at an accelerating voltage of 15 kV. The samples were dried at ambient temperature and vacuum-sputtered with Pt of average size 3 nm. Wide-angle X-ray powder scattering (Rigaku D/max-2500) was used to characterize the crystalline phases. The crystalline inorganic-oxide content of the composite spheres was determined by TGA (Perkin Elmer analyzer Pyris 1) in the temperature range 30–800 °C in nitrogen at a heating rate of 10 °C min^{-1}. Elemental analysis was carried out with a Flash EA-1112 apparatus. FTIR spectra were recorded on a Bruker Equinox 55 spectrometer with samples pressed into KBr pellets. Nitrogen adsorption was performed on a Micrometritics ASAP 2020M surface area and porosity analyzer. XPS data were obtained on an ESCALab220i-XL electron spectrometer from VG Scientific with 300-W $Al_{K\alpha}$ radiation. The base pressure was about 3×10^{-9} mbar. The binding energies were referenced to the C1s line at 284.8 eV from adventitious carbon.

Acknowledgements

[1] W. Schärtl, *Adv. Mater.* **2000**, *12*, 1899, and references therein.
[2] F. Caruso, *Adv. Mater.* **2001**, *13*, 11, and references therein.
[3] R. A. Caruso, A. Susha, F. Caruso, *Chem. Mater.* **2001**, *13*, 400.
[4] K. H. Rhodes, S. A. Davis, F. Caruso, B. Zhang, S. Mann, *Chem. Mater.* **2000**, *12*, 2832.
[5] I. Pastoriza-Santos, B. Schöler, F. Caruso, *Adv. Funct. Mater.* **2001**, *11*, 122.
[6] C. Schüler, F. Caruso, *Biomacromolecules* **2001**, *2*, 921.
[7] A. J. Khopade, F. Caruso, *Nano Lett.* **2002**, *2*, 415.
[8] F. Caruso, M. Spasova, A. Susha, M. Giersig, R. A. Caruso, *Chem. Mater.* **2001**, *13*, 109.
[9] F. Caruso, R. A. Caruso, H. Möhwald, *Science* **1998**, *282*, 1111.
[10] L. Wang, T. Sasaki, Y. Ebina, K. Kurashima, M. Watanabe, *Chem. Mater.* **2002**, *14*, 4827.
[11] M. R. Hoffmann, S. T. Martin, W. Choi, D. W. Bahnemann, *Chem. Rev.* **1995**, *95*, 69.
[12] S. J. Kim, S. D. Park, Y. H. Jeong, *J. Am. Ceram. Soc.* **1999**, *82*, 927.
[13] K.-J. Kim, K. D. Benkstein, J. van de Lagemaat, A. J. Frank, *Chem. Mater.* **2002**, *14*, 1042.
[14] M. A. Peña, J. L. G. Fierro, *Chem. Rev.* **2001**, *101*, 1981.
[15] M. T. Buscaglia, M. Viviani, Z. Zhao, V. Buscaglia, P. Nanni, *Chem. Mater.* **2006**, *18*, 4002.
[16] J. Moreno, J. M. Dominguez, A. Montoya, L. Vicente, T. Viveros, *J. Mater. Chem.* **1995**, *5*, 509.
[17] B. Schlarb, M. G. Rau, S. Haremz, *Prog. Org. Coat.* **1995**, *26*, 207.
[18] J. E. G. J. Wijnhoven, W. L. Vos, *Science* **1998**, *281*, 802.
[19] S. Roberts, *Phys. Rev.* **1949**, *76*, 1215.
[20] Q. Peng, Y. Dong, Y. Li, *Angew. Chem. Int. Ed.* **2003**, *42*, 3027.
[21] T. Nakashima, N. Kimizuka, *J. Am. Chem. Soc.* **2003**, *125*, 6386.
[22] C. Guo, Y. Cao, S. Xie, W. Dai, K. Fan, *Chem. Commun.* **2003**, 700.
[23] A. Imhof, *Langmuir* **2001**, *17*, 3579.
[24] M. Yang, J. Ma, C. Zhang, Z. Yang, Y. Lu, *Angew. Chem.* **2005**, *117*, 6885; *Angew. Chem. Int. Ed.* **2005**, *44*, 6727.

FULL PAPERS

[25] S. Ding, C. Zhang, M. Yang, X. Qu, Y. Lu, Z. Yang, *Polymer* **2006**, *47*, 8360.

[26] Z. Yang, Z. Niu, Y. Lu, Z. Hu, C. C. Han, *Angew. Chem.* **2003**, *115*, 1987; *Angew. Chem. Int. Ed.* **2003**, *42*, 1943.

[27] M. Yang, J. Ma, Z. Niu, X. Dong, H. Xu, Z. Meng, Z. Jin, Y. Lu, Z. Hu, Z. Yang, *Adv. Funct. Mater.* **2005**, *15*, 1523.

[28] J. Y. Lee, J. H. Lee, S. H. Hong, Y. K. Lee, J. Y. Choi, *Adv. Mater.* **2003**, *15*, 1655.

[29] C. C. Wang, J. Y. Ying, *Chem. Mater.* **1999**, *11*, 3113.

[30] R. Ayouchi, F. Martín, J. R. Ramos-Barrado, D. Leinen, *Surf. Interface Anal.* **2000**, *30*, 565.

[31] M. Gopal, W. J. Moberly Chan, L. C. De Jonghe, *J. Mater. Sci.* **1997**, *32*, 6001.

[32] E. Scolan, C. Sanchez, *Chem. Mater.* **1998**, *10*, 3217.

[33] K.-N. P. Kumar, K. Keizer, A. J. Burggraaf, T. Okubo, H. Nagamoto, S. Morooka, *Nature* **1992**, *358*, 48.

[34] S. Wada, T. Tsurumi, H. Chikamori, T. Noma, T. Suzuki, *J. Cryst. Growth* **2001**, *229*, 433.

[35] J. Q. Qi, L. T. Li, Y. L. Wang, Z. L. Gui, *J. Cryst. Growth* **2004**, *260*, 551.

[36] V. R. Calderone, A. Testion, M. T. Buscaglia, M. Bassoli, C. Bottino, M. Viviani, V. Buscaglia, P. Nanni, *Chem. Mater.* **2006**, *18*, 1627.

[37] E. A. Barringer, H. K. Bowen, *Langmuir* **1985**, *1*, 420.

[38] R. A. Spurr, H. Myers, *Anal. Chem.* **1957**, *29*, 760.

[39] A. J. van der Vlies, G. Kishan, J. W. Niemantsverdriet, R. Prins, Th. Weber, *J. Phys. Chem. B* **2002**, *106*, 3449.

[40] K. Wu, E. G. Wang, Z. X. Cao, Z. L. Wang, X. Jiang, *J. Appl. Phys.* **2000**, *88*, 2967.

[41] M. Niederberger, G. Garnweitner, N. Pinna, M. Antonietti, *J. Am. Chem. Soc.* **2004**, *126*, 9120.